Recent Studies of Subsonic Vortex Lift Including Parameters Affecting Stable Leading-Edge Vortex Flow

John E. Lamar*
NASA Langley Research Center, Hampton, Va.

Various subsonic configurations that develop vortex lift are examined herein. Comparisons are made with data and the combination of direct and indirect edge forces through use of the suction analogy. For most configurations, the use of the indirect or augmented vortex lift leads to improved agreement with data. The studies conducted showed that it is possible for the leading-edge vortex to exhibit sudden enlarging on a cropped wing and for the wing longitudinal aerodynamic characteristics not to show the effect. It was further found that the distributions of leading-edge suction correlate well with the maintenance of vortex-flow aerodynamic characteristics. Lastly, an approximate method is presented for relating the initial value of circulation and axial velocity of the leading-edge shed vortex to the wing geometry.

Nomenclature

A = aspect ratio
b = wingspan
C_D = drag coefficient, drag/$q_\infty S_{\text{ref}}$
C_L = lift coefficient, lift/$q_\infty S_{\text{ref}}$
ΔC_L = C_L increment associated with augmented-vortex lift
C_m = pitching-moment coefficient about reference point that is located at $c_{\text{ref}}/4$ unless otherwise stated, pitching moment/$q_\infty S_{\text{ref}} c_{\text{ref}}$
C_N = normal-force coefficient, normal force/$q_\infty S_{\text{ref}}$
C_S = leading-edge suction-force coefficient, $K_{v,le}\sin^2\alpha$
c = streamwise chord
$\bar{c}$ = characteristic length used in determination of $\bar{K}_{v,se}$
dF_S = differential leading-edge suction force (Fig. 2)
K_p = potential-lift factor, $\partial(C_{N,p})/\partial(\sin\alpha\cos\alpha)$
$K_{v,le}$ = leading-edge vortex-lift factor, ∂[2 (leading-edge suction force from one edge)/$q_\infty S_{\text{ref}}$]/$\partial\sin^2\alpha$
$K_{v,se}$ = side-edge vortex-lift factor, ∂[2(side-edge suction force from one edge)/$q_\infty S_{\text{ref}}$]/$\partial\sin^2\alpha$
$\bar{K}_{v,se}$ = augmented vortex-lift factor, $[K_{v,le}/(b/2)\sec\Lambda]\bar{c}$
$k(\alpha)$ = pitch of helical vortex along the leading edge
LE = leading edge
l = distance along leading edge from apex
M_∞ = freestream Mach number
NF = normal force
q_∞ = freestream dynamic pressure
S = surface area
SE = side edge
U = freestream velocity
V_{ax} = axial velocity along helical vortex centerline
w_{net} = sum of induced downwash and $U\alpha$ at $\alpha = 1$ rad
$\bar{w}$ = average value of induced downwash at $\alpha = 1$ rad
α = angle of attack
α_{BD} = angle of attack for leading-edge vortex breakdown
α_D = departure angle of attack
Γ = circulation
$\bar{\Gamma}$ = average value of Γ along the leading edge
δ_f = leading-edge flap angle, positive upward
η = fraction spanwise coordinate – 0 at root, 1 at right wingtip
η_{cp} = fractional semispan location of panel total normal force
ρ = density of fluid
Λ = leading-edge sweep angle, positive for sweepback
λ = taper ratio, c_t/c_r
Ω = trailing-edge sweeep angle, positive for sweepback

Subscripts

le = leading edge
p = potential or attached flow
r = root
ref = reference; for S, true wing area; for c, mean geometric chord
t = tip
te = trailing edge
vle = vortex effect at leading edge
vse = vortex effect at side edge

Introduction

IN the design and analysis of high-speed aircraft, a detailed knowledge of the effects of flow separation is required, particularly with regard to critical wing loads, maximum lift, and the stability and performance at various off-design conditions. One class of separation which is often encountered is around the leading and side edges. The resulting vortex-flow aerodynamics are important with regard to aero/structural tradeoffs and are being increasingly utilized to improve the maneuvering capability of fighters.

Polhamus introduced a method for estimating the direct vortex lift generated from the leading edges of delta wings[1] and later extended it to other pointed wings.[2] This method employs a suction analogy and more recently has been utilized to estimate the direct vortex lift from the side edges.[3-6] Comparisons with data are offered for rectangular wings using these direct vortex lifts.

In addition to these direct lifts, experimental evidence from both overall force and flow visualization indicate the existence of an indirect or "free" vortex lift. This lift is called the augmented contribution and was introduced and quantified in Ref. 7. A large portion of this paper is devoted to examining and refining this contribution, which has led to improved lift agreement for various wings.

Furthermore, the analysis leading to the augmented contribution provided an opportunity to examine the relationship between the wing geometry and the initial condition of cir-

Presented as Paper 76-414 at the AIAA 9th Fluid and Plasma Dynamics Conference, San Diego, Calif., July 14-16, 1976; submitted Aug. 27, 1976; revision received Aug. 31, 1977.

Index categories: Aerodynamics; Subsonic Flow; Configuration Design.

*Aeronautical Research Scientist. Member AIAA.

culation and axial velocity that exist near the center of the shed vortex system core. Some of the results are discussed.

Another idea, which similarly deals with the relationship between wing geometry and the shed vortex system, also introduced in Ref. 7, is utilized with the view toward finding the important geometric parameters affecting stable leading-edge vortex flow aerodynamic situations. This idea involves the potential flow leading-edge suction-force distribution and is employed to try to improve the vortex lift on a planform that normally develops very little of the theoretically available vortex lift.

Vortex Lift

Rectangular-Wing Root-Bending Moment

With the generalization of the suction analogy to include wings having streamwise side edges, opportunities open for the estimation of vortex flow contributions to lift, pitching moment, and root-bending moment for these more arbitrary planforms. Reference 3 documents C_L and C_m comparisons for a series of wings including rectangular ones. Figure 1 presents the C_N-α comparison from Ref. 3 for an $A=1$ rectangular wing and introduces a procedure for estimating the root-bending moment and finding the effective spanwise centroid of the loading. The procedure is to sum half the potential normal force acting through its centroid with the leading-edge and side-edge vortex flow normal forces acting through the spanwise centroid and the tip, respectively. This sum is divided by the above normal forces at that angle of attack to determine an effective spanwise centroid. It is compared with experimentally determined ones (obtained from the results of Ref. 8) over an α range for the three different rectangular wings shown in Fig. 1.

For all wings considered, the experimental centroids are outboard of the potential flow ones and generally inboard of those obtained by the preceding procedure. (This is expected since the vortex normal forces are assumed to act along the edges.) The latter is only untrue when α exceeds that angle for which the leading-edge vortex flow no longer reattaches on the wing. Hence, the procedure outlined for calculating an effective span load centroid can be considered generally conservative for sharp-edge rectangular wings with leading-edge reattached vortex flows.

This same procedure could also be applied to other planforms and should similarly yield conservative results. (See Ref. 9 for delta wing examples.)

Augmented Lift Effects

General

The concept of the augmented vortex lift is developed in Ref. 7 and, hence, only will be summarized herein. Augmented vortex lift is thought of as the result of the leading-edge vortex system passing over an area downstream of the leading-edge tip as shown in Fig. 2. This vortex lift is only indirectly related to the edge forces, whereas the vortex lifts arising along the leading and side edges are directly related. The augmented lift was originally quantified for cropped-delta wings, but the formulation has been used for other cropped and pointed wings as shown in Ref. 7. The formulation for the associated lift coefficient increment is

$$\Delta C_L = \bar{K}_{v,se} \left| \sin\alpha \right| \sin\alpha\cos\alpha \tag{1}$$

where

$$\bar{K}_{v,sec} = \left(\frac{K_{v,le}}{(b/2)\sec\Lambda}\, \tilde{c} \right) \tag{2}$$

and $\tilde{c}$ = characteristic length, usually the streamwise distance from the leading-edge tip to the trailing-edge apex. (Can be positive or negative.) One of the purposes of this paper is to determine what refinements are necessary in the employment of $\tilde{c}$ for various angles of attack. This will be taken up with a cropped-arrow wing, after which applications will be made to 45-deg swept wings with a variety of tip chord and trailing-edge arrangements. However, first C_L and C_m comparisons will be made for two-pointed wings using the original $\tilde{c}$ definition.

Pointed Wing

Reference 10 presents data and theoretical comparisons for 74-deg swept delta, arrow, and diamond wings over a Mach range from 0.2 to 0.8. The delta wing data are well estimated with the combination of potential flow (0% leading-edge suction) and the leading-edge vortex flow, whereas those for the arrow and diamond wing are not. However, incorporating the augmented vortex lift produces improved agreement with

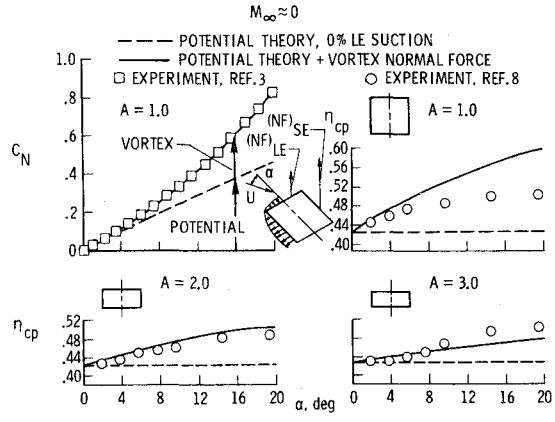

Fig. 1 Effect of vortex normal force on rectangular wing spanwise load center, $M_\infty \approx 0$.

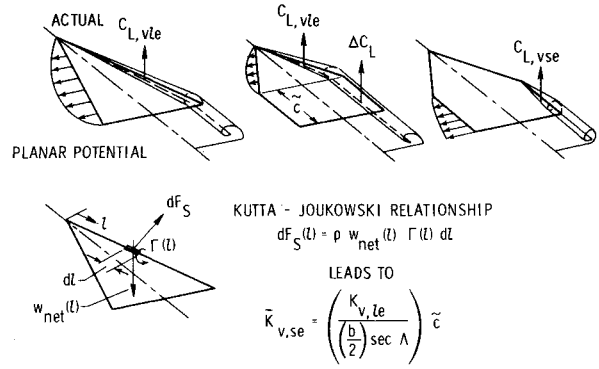

Fig. 2 Concept of augmented vortex lift.

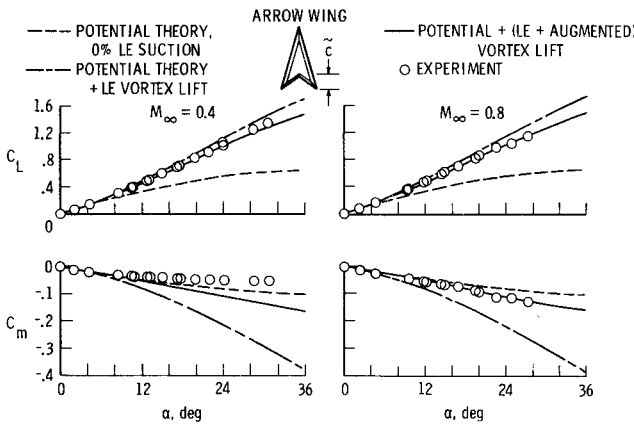

Fig. 3 Effect of Mach number on augmented vortex lift and pitch, arrow wing.

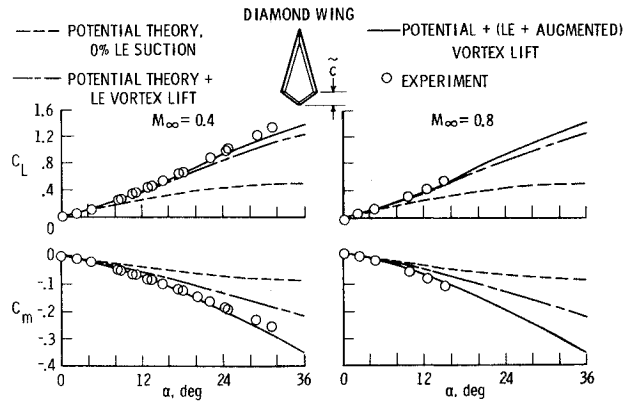

Fig. 4 Effect of Mach number on augmented vortex lift and pitch, diamond wing.

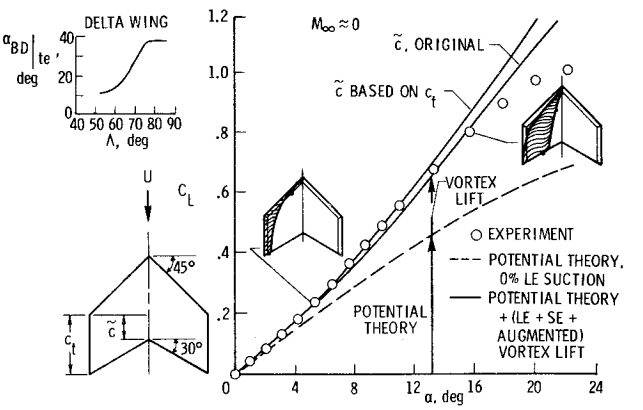

Fig. 5 Effect of $\tilde{c}$ definition on estimated C_L, $M_\infty \approx 0$.

the C_L and C_m data as seen in Figs. 3 and 4 for $M_\infty = 0.4$ and 0.8. Note especially the smaller sensitivity of the diamond wing C_m variation with Mach number. Also, note that due to the slenderness of these wings, the theoretical curves are almost identical for each wing over its entire subsonic speed regime.

Reference 11 also treats these pointed wings, but the method presented therein incorporates a slender wing theory with "ceiling" limits on both the attached and vortex flow lifts to account for nonslender aerodynamic behavior. In addition, equivalent delta wings are introduced to aid in the calculation of the arrow and diamond wing attached and vortex flow aerodynamic forces. With these assumptions, this method did provide remarkably good agreement with the arrow and diamond wing data.

It should be noted that the method previously discussed, which included the augmented vortex lift, does not employ "ceiling" limits or equivalent delta wings; instead, it employs a physical flow reasoning. The reasoning for an augmented lift is easier to understand when applied to a diamond wing or one with additional area aft of the leading-edge tip than when applied to arrow-type wings. However, the negative value of augmentation for these wings should be thought of as a lack of complete flow reattachment due to trailing-edge notching.

This notching effect is well documented by the transonic longitudinal load distribution of a highly swept and tapered cropped-arrow wing-body combination in Ref. 12. The distribution shows a sudden loss in lift just aft of the trailing-edge apex. This integrated loss is likened to the negative value of augmented vortex lift discussed previously. Reference 12 employed the augmented lift concept for this combination and reported improved agreement with the data.

Cropped-Wing Application

Figure 5 shows the lift characteristics for a sharp-edged cropped-arrow wing at $M_\infty \approx 0$. Although generally good agreement between the data and the present method is achieved with the original definition of $\tilde{c}$, for $\alpha \leq 16$ deg, some disparagy is noted for 8 deg $< \alpha <$ 14 deg. The inserted oil-flow sketches show that the leading-edge vortex reattachment line occurs near the wingtip at low angles of attack, whereas at the higher ones, the reattached line is more inboard. This inboard movement associated with the increase in vortex size is well known and documented for wings having a wide range of leading-edge sweep angles. Since all vortex lift terms increase in proportion to $|\sin\alpha|\sin\alpha\cos\alpha$, thereby making the most contribution at the "higher" angles of attack, the $\tilde{c}$ associated with the more inboard reattachment line – the original one – has been used as being representative of the augmented vortex lift capability of this wing. However, the preceding leads to an underestimation of the C_L data, whereas using $\tilde{c}$ based on the low-angle-of-attack reattachment line ($\tilde{c} = c_t$) results in better agreement and an upper bound.

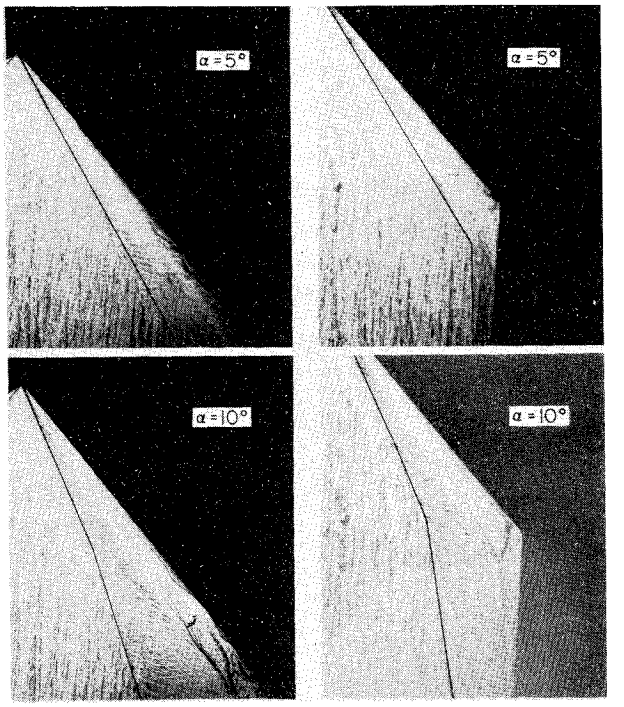

Fig. 6 Oil-flow photographs for 45-deg delta and cropped delta ($\lambda = 0.5$), $\alpha = 5$ and 10 deg, $M_\infty \approx 0$.

There are two basic reasons why the data could fall below the present method ($\tilde{c}$ original) estimates: 1) vortex breakdown or sudden enlargment occurs ahead of the trailing edge; or 2) the vortex system gets so large that it is unable to completely reattach and recover all the direct and indirect vortex forces. The insert on Fig. 5, taken from Ref. 13, shows the variation of $\alpha_{BD|te}$ with Λ for delta wings. With extrapolation to the $\Lambda = 45$ deg delta wing, $\alpha_{BD|te}$ is postulated to be ≈ 10 deg, even though this reference reported that the vortex was not visible at any α for this wing.

Examination of the oil-flow photographs for the flat 45-deg sharp-edged delta wing shown in Figs. 6 and 7 leads to the observation that the reattachment line – its approximate position inked in – undergoes flairing ahead of the trailing edge for $\alpha \geq 10$ deg. Reference 14 relates a bending, herein called flairing, of the secondary separation line to vortex bursting; however, figures from the reference show that flairing has also occurred for the primary reattachment line when vortex bursting is present. Hence, if the reattachment line flairs in the present oil-flow photographs, at least a sudden enlargement of the primary vortex is taken to have occurred. For comparison, oil-flow photographs for a flat 45-deg cropped-delta wing having sharp edges and $\lambda = 0.5$ are

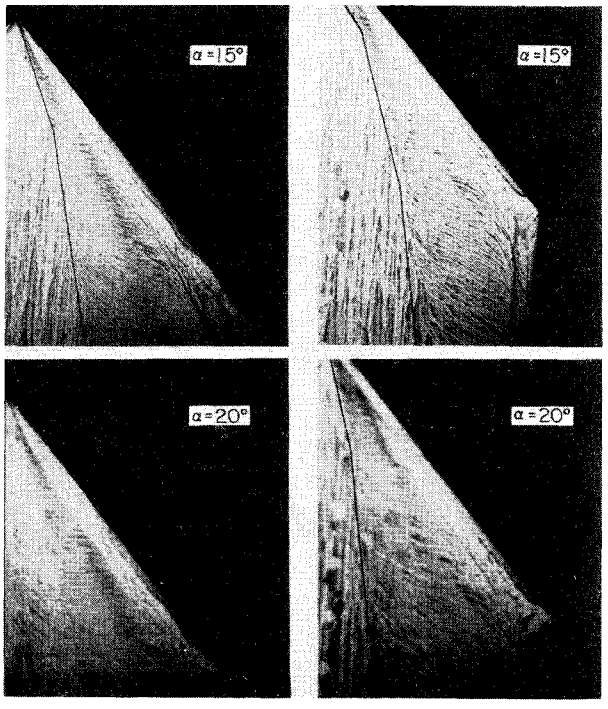

Fig. 7 Oil-flow photographs for 45-deg delta and cropped delta ($\lambda = 0.5$), $\alpha = 15$ and 20 deg, $M_\infty \approx 0$.

presented. The inked-in approximate locations for the reattachment lines behave similarly on the delta part of the cropped wing. However, Ref. 7 showed that for this wing it generates the estimated vortex lift and pitching moment to angles of attack >15 deg. Hence, it would appear that although the leading-edge vortex was suddenly enlarging, the influence of the side edge provides 1) additional area for the rotating flow to act over and/or 2) a favorable pressure gradient or increased circulation associated with the tip flow which reenergizes the leading-edge flow leading to a stable vortex flow aerodynamic situation. The preceding may also reduce the helix angle.

The angle of attack at which the data begin to fall below the present method, for whatever reason, is herein called the departure angle and is denoted by α_D. For the cropped-delta wing of Figs. 6 or 7, $\alpha_D \approx 16$. From Ref. 13, it can be seen that α_{BDlie} and the definition of α_D would correlate reasonably well for delta wings having $\Lambda \leq 77.5$ deg, for which bursting was observable.

It should be noted that the maximum augmented vortex lift for a cropped-diamond wing will occur using the original $\tilde{c}$ value; hence, refinements are investigated neither for this class of wing nor for the diamond wing.

Forty-Five Degree Swept Wings

One reason for the interest in the 45-deg cropped arrow is that current high-performance fighter aircraft of both the U.S.A. and USSR have leading-edge sweep angles and taper ratios which put them in this general class of planform as shown in Fig. 8. Another reason is that more slender wings have already received considerable attention in the literature. To further investigate the effect of taper ratio and the trailing-edge sweep angle on the C_L characteristics of swept wings, a systematic analytical and wind-tunnel study was conducted[15] and selected results, $\alpha \approx 8$ deg and 16 deg, are presented in Fig. 9. An interesting observation is that at each angle of attack, the estimated vortex lift increment (for $\tilde{c}$ original) is essentially constant even though λ and Ω vary widely. Furthermore, good agreement between theory and data is seen for the trailing-edge sweep case at both angles of attack. Also note here, as in Fig. 5, that at the lower angles of attack $\tilde{c} = c_t$

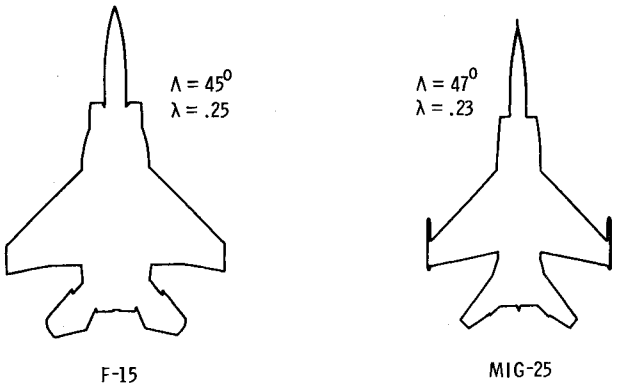

Fig. 8 Current fighter aircraft.

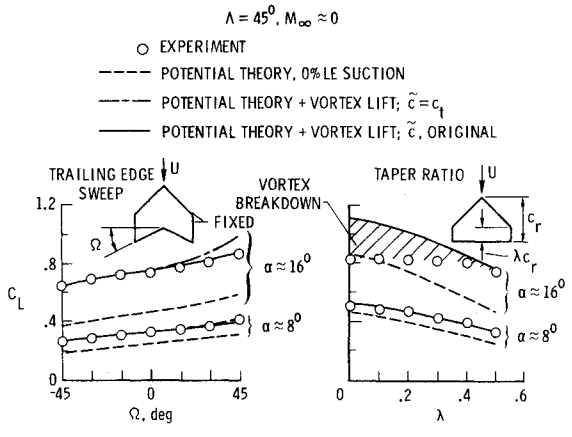

Fig. 9 Effect of aft area on swept wing vortex lift, $\Lambda = 45$ deg, $M_\infty \approx 0$.

provides a better estimate of the augmented vortex lift for the highly notched cropped-arrow wings. The taper ratio series shows good agreement between data and theory at $\alpha \approx 8$ deg followed by a falloff in the measured C_L with decreasing λ at $\alpha \approx 16$ deg. Oil-flow studies show that with decreasing λ more of the flat wing leading edge experiences stalled flow at the "higher" angles of attack with a significant relative enlargement of the aft area bounded by the reattachment line and the leading edge. Ref. 7 makes an observation about the α_D for this taper ratio series of cropped-delta wings in conjunction with its distribution of local leading-edge suction forces. This will be discussed in detail later.

Unswept Leading Edge

It is possible for augmented vortex lift to be experienced on unswept wings of low or moderate aspect ratio if they have significant side edges and a swept trailing edge, as typified by the configuration shown in Fig. 10. An interesting note for the swept-back wing is that in the wrapup of the shed vortex system the portion produced by the leading edge comes toward the center of the system, whereas, the portion produced by the side edge moves toward the periphery. Thus, it is only the leading-edge vortex system which was used in the swept-wing augmented vortex lift. However, for the unswept leading edge the leading- and side-edge shed-vortex systems remain separate. Hence, it is the side-edge portion which lies near the center of the vortex system and provides the augmentation for this class of wing. The C_L data on Fig. 10 indicate that there is more lift measured than estimated by the combination of potential lift (0% leading-edge suction) and leading- and side-edge vortex lift. Moreover, the technique used for the leading-edge augmented vortex lift cannot be applied for this wing and, thus, the estimates for the data are lower over part of the angle-of-attack range as would be expected if augmentation were present but not taken into

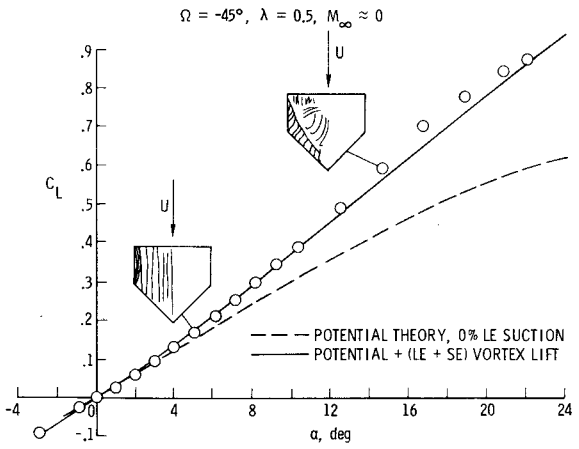

Fig. 10 Effect of augmented vortex lift on wing with unswept leading edge.

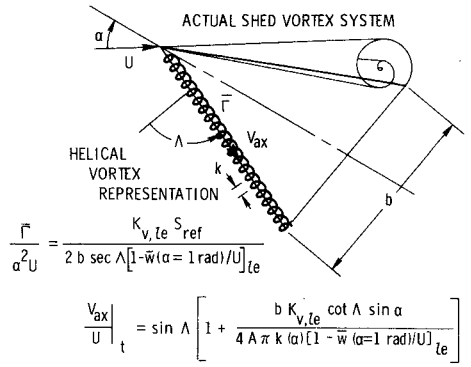

Fig. 11 Parameters affecting vortex core axial velocity based on a helical vortex representation.

account. Even though this augmented vortex lift concept cannot be employed directly, it is possible that the concept can be used to estimate the circulation Γ of the system. However, this estimated circulation is not an averaged value as used previously and as appears in Ref. 7 but the one at the trailing-edge tip. For this wing Γ is determined to be

$$\left.\frac{\Gamma}{\text{length}}\right|_{te,t} \approx \frac{U\sin\alpha}{2}$$

The oil-flow sketch inserts show the inboard movement of the side-edge vortex flow with increasing angle of attack as would be expected.

Stable Leading-Edge Vortex Situations

Various authors (for example, see Refs. 16-18) have written about the determination of the stability of leading-edge shed vortex systems. These authors are generally forced to treat the shed vortex problem in an isolated sense and some do so without including the effects of viscosity while others do. These treatments, by necessity, require certain assumptions concerning the initial conditions of the core region. They do not relate the resulting solution to any particular vortex generating wing. Using the concept of the augmented vortex lift and the fact that the leading-edge shed system surrounds the core, it seems feasible to relate, at least on an average basis, the wing geometry to some of the initial conditions, such as circulation and axial velocity, needed for a vortex stability solution. The circulation has already been considered in Ref. 7 (given on Fig. 13). Now the axial velocity will be determined based on the helical vortex representation shown in Fig. 11. The helical vortex starts at the apex and terminates

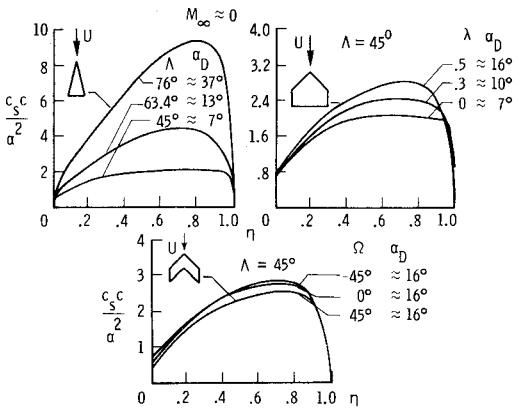

Fig. 12 Leading-edge suction distributions and α for departure for uncambered wings.

at the tip indicative of the region which is assumed to feed the shed vortex system. The radius of the helix is assumed to be a small fraction of the span in keeping with the original concept of the suction analogy.[1] Upon solving for the axial velocity component along the center of the helix – along the wing leading edge – an integral results that can be evaluated over the limits previously mentioned. Employing the average circulation from the augmented vortex lift concept leads to an axial velocity to freestream velocity ratio at the wingtip of

$$\left.\frac{V_{ax}}{U}\right|_t = \sin\Lambda\left[1 + \frac{bK_{v,le}\cot\Lambda\sin\alpha}{4A\pi k(\alpha)\,[1-\bar{w}(\alpha=1\text{rad})/U]_{le}}\right] \qquad (3)$$

Some of these terms can be specified from geometry, Λ, b, A, and α; whereas, others must be solved for using a potential flow computer program, $K_{v,le}$ and $\bar{w}$; and the variation and magnitude of the pitch of the helix with angle of attack $k(\alpha)$ must be determined experimentally, perhaps from surface oil flows near the apex.

As an illustration of the variation of $(V_{ax}/U)|_t$ with the geometrical parameters, three delta wings having sweep angles of 45, 63.4, and 76 deg were selected for study. The A for delta wings is given by 4 cotΛ and with the assumptions of $b=2$ and $k(\alpha)$ a constant for all three wings leads to

$$\left.\frac{V_{ax}}{U}\right|_t = \sin\Lambda\left[1 + \frac{K_{v,le}\sin\alpha}{8\pi k(\alpha)\,[1-\bar{w}(\alpha=1\text{rad})/U]_{le}}\right] \qquad (4)$$

Employing the necessary potential flow solutions results in

$$\left.\frac{V_{ax}}{U}\right|_t = \begin{cases} 0.707 + 0.0146\sin\alpha/k(\alpha) & (\Lambda = 45\text{ deg}) \\ 0.894 + 0.0169\sin\alpha/k(\alpha) & (\Lambda = 63.4\text{ deg}) \\ 0.970 + 0.0178\sin\alpha/k(\alpha) & (\Lambda = 76\text{ deg}) \end{cases} \qquad (5)$$

From Eq. (3) and the assumptions made, it can be seen that $(V_{ax}/U)|_t$ increases with increasing Λ as one might expect. Hence, there is at least one qualitative check on the equation. An interesting observation about the trend of the numbers in the second term that appears in Eq. (5) is that they result due to the dominance of the sin Λ multiplier. This dominance causes a reversal in the variation of the second term in Eq. (4) with increasing Λ. For $k(\alpha) \approx 0.005$ $(b/2)$ and $\alpha \geq 6$ deg, $(V_{ax}/U)|_t > 1$ for all preceding Λ. Thus, it is consistent with Ref. 17.

Another possible influence on the leading-edge vortex stability is the potential flow distribution of the local leading edge-suction force as discussed in Ref. 7. This should be more properly identified as leading-edge vortex flow stabilized situations in which even if the vortex suddenly enlarges, the rotational flow still causes reattachment and the overall

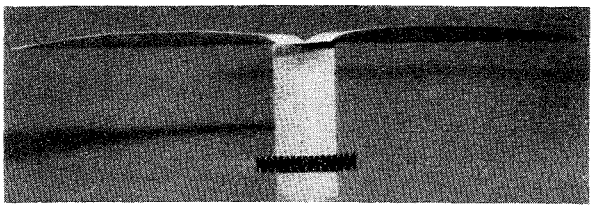

a) Front view

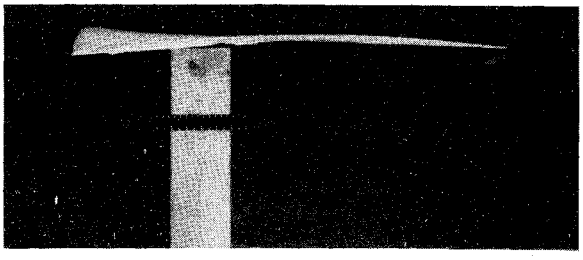

b) ¾ front view

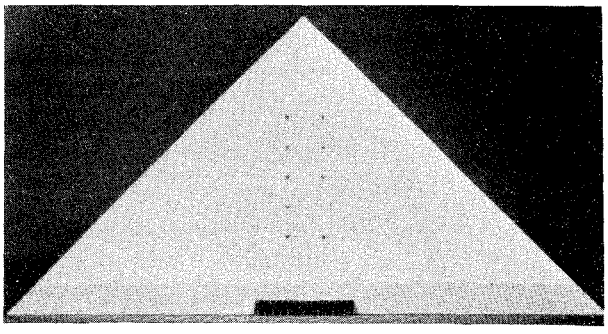

c) Plan view

Fig. 13 Linearly twisted 45-deg delta wing.

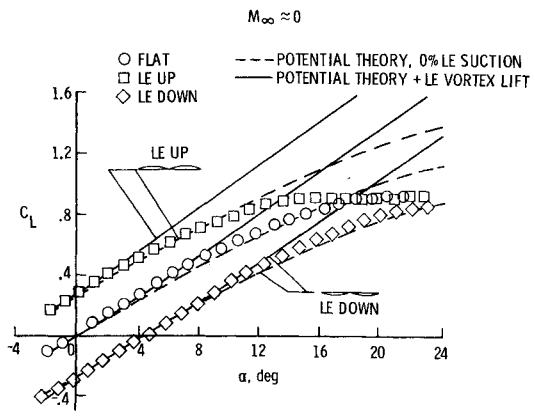

Fig. 14 Lift characteristics for 45-deg delta wing, flat and linearly twisted ("bat wing"), $M_\infty \approx 0$.

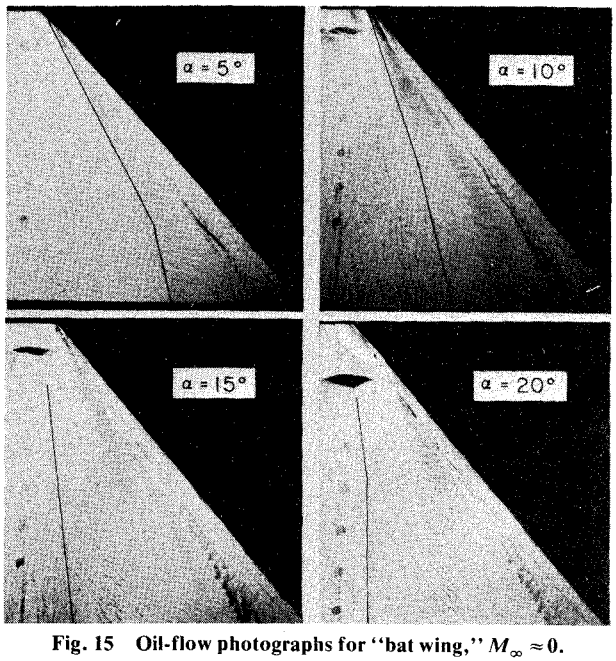

Fig. 15 Oil-flow photographs for "bat wing," $M_\infty \approx 0$.

longitudinal forces and moments do not reflect a change in their growth with angle of attack. Figure 12 shows $c_s c/\alpha^2$ spanwise distributions for the preceding delta wings as well as the 45-deg swept-wing taper ratio and trailing-edge sweep series. In addition to the change in amplitude with wing geometry, the distributional variations are worthy of note. In particular, if α_D is used as a gage of a vortex stable situation, then the larger the peak value of the $c_s c/\alpha^2$ and the more outboard its location correlate well with increasing α_D. This is particularly apparent for increasing the taper ratio on the 45-deg delta wing. The addition of a significant side edge seems to be important not only in "improving" the $c_s c/\alpha^2$ potential flow distribution, but physically enhancing the attainable vortex lift by either stabilizing the leading-edge vortex, reducing the helix angle, or providing additional area onto which reattachment can occur. Furthermore, upon retaining the tip chord associated with the $\lambda = 0.5$ cropped delta and the leading-edge length, trailing-edge sweep variations result in only a small change in the $c_s c/\alpha^2$ peak value or distribution over the wide Ω range shown in Fig. 12. The accompanying α_D results, all ≈ 16 deg, further attest to the correlation between the $c_s c/\alpha^2$ distribution and the attainable vortex lift.

It has already been noted that the 45-deg delta wing has a low value of α_D as well as a "poor" $c_s c/\alpha^2$ distribution. Therefore, an attempt to improve the attainable vortex lift on this wing by twisting it was investigated. An initial study showed the linear incidence varying from 0 deg at the root to ≈ 12 deg at the tip would provide a more outboard peak of the $c_s c/\alpha^2$ distribution over a wide C_L range. This incidence distribution is opposite to that associated with attached flow solutions because they reduce the loading outboard, whereas the solution sought would increase the load and local suction force. This solution was to emphasize the separated flow, not the attached flow aerodynamics, and resulted in an unconventional configuration which was constructed and wind-tunnel tested. Figure 13 shows several views of the model including a head on one in which it resembles a "bat wing."

Figure 14 presents the C_L data for the flat 45-deg delta wing and the "bat wing" in its upright (LE up) and inverted (LE down) position along with the appropriate theoretical estimates. It is obvious that the theoretical gains were not realized in the upright position. The reason the "bat wing" design failed is probably due to the enlarged vortex – relative to the flat delta – at all angles of attack not having enough aft area to reattach onto. "Bat wing" oil-flow photographs are given in Fig. 15 and can be compared with the flat delta ones given in Figs. 6 and 7.

It is interesting to note from Fig. 14 that for the inverted case, more of the vortex lift is realized despite its leading-edge suction distribution not being favorable. It appears, therefore, for this planform the benefit of shifting the vortex lift forward, such that more area for reattachment is available, outweighs the stabilizing influence of the suction distribution.

Another experimental method was also tried to improve the 45-deg delta wing α_D or C_L characteristics. It was based on studies performed at ONERA for a 70-deg delta-type wing. This method produced significant C_L improvements at α's associated with takeoff and landing. The improvements came from deflecting the leading-edge flap up.

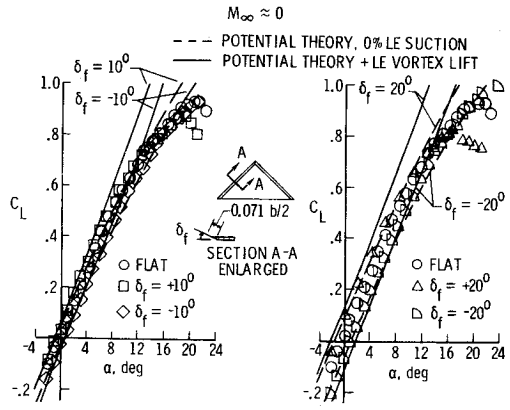

Fig. 16 Effect of LE flap deflection on 45-deg delta wing lift characteristics, $M_\infty \approx 0$.

The available data were only for flap settings of ±20 deg; hence, the wind-tunnel study undertaken in support of the 45-deg delta wing program included not only ±20 deg, but ±10 deg deflections as well, to ascertain the flap effectiveness. The experimental results are shown in Fig. 16 and the data confirm that, by deflecting the leading-edge flap upward, there are C_L improvements also for this delta wing; however, for both deflection angles, most of the beneficial effect is gone by $\alpha \approx 12$ deg. The $\delta_f = +10$ deg results more nearly reach the local theoretical maximums than do the $\delta_f = +20$ deg ones. Deflecting the leading-edge downward leads to a higher maximum C_L because of the improved onflow for both values of δ_f, similar to the trend for the inverted "bat wing."

Conclusions

Various configurations which develop vortex lift have been analyzed herein and the conclusions drawn are as follows:

1) The spanwise centroid of normal force for a series of rectangular wings can be conservatively estimated by including the potential flow and leading- and side-edge vortex flow normal forces. This procedure is valid as long as the leading-edge separated flow reattaches onto the wing.

2) Including the augmented or indirect vortex flow aerodynamic effect leads to generally improved agreement with experimental data.

3) The characteristic length in the augmented lift term is a function of angle of attack, as demonstrated for a cropped arrow. At low angles, the length is approximately equal to the tip chord, whereas at higher angles, it is more nearly the streamwise distance from the leading-edge tip to the trailing-edge apex.

4) It is possible for the leading-edge vortex to exhibit sudden enlarging on the wing and for the wing longitudinal aerodynamic characteristics not to show the effect. This occurs when the wing has a sufficient side edge to provide a) additional area for the rotating flow to act over and/or b) a favorable pressure gradient or increased circulation associated with the tip flow. The preceding may also reduce the helix angle.

5) The effect of side-edge length on the 45-deg cropped-delta wing studied is more important in maintaining the vortex flow lift characteristics than is taper ratio or trailing-edge sweep angle.

6) The distribution of the leading-edge suction force has been found to correlate well with the maintenance of vortex flow aerodynamic characteristics on a variety of planforms. Those planforms that have suction peak values occurring nearer the wing tip are the ones that retain the vortex flows to higher angles of attack.

A method has been presented by which an estimate of the axial velocity in the core of the leading-edge shed vortex at the tip can be related to wing geometry. This velocity, along with an estimate of the circulation, developed previously, may be of use as initial conditions in an examination of the stability of these vortices.

References

[1] Polhamus, E. C., "A Concept of the Vortex Lift of Sharp-Edge Delta Wings Based on a Leading-Edge-Suction Analogy," NASA TN D-3767, 1966.

[2] Polhamus, E. C., "Charts for Predicting the Subsonic Vortex-Lift Characteristics of Arrow, Delta, and Diamond Wings," NASA TN D-6243, 1971.

[3] Lamar, J. E., "Extension of Leading-Edge Suction Analogy to Wings with Separated Flow Around the Side Edges at Subsonic Speeds," NASA TR R-428, 1974.

[4] Bradley, R. G., Smith, C. W., and Bhateley, I. E., "Vortex-Lift Prediction for Complex Wing Planforms," *Journal of Aircraft*, Vol. 10, June 1973, pp. 379-381.

[5] Lamar, J. E., "Prediction of Vortex Flow Characteristics of Wings at Subsonic and Supersonic Speeds," *Journal of Aircraft*, Vol. 13, July 1976, pp. 490-494.

[6] Lamar, J. E. and Gloss, B. B., "Subsonic Aerodynamic Characteristics of Interacting Lifting Surfaces with Separated Flow Around Sharp Edges Predicted by a Vortex-Lattice Method," NASA TN D-7921, 1975.

[7] Lamar, J. E., "Some Recent Applications of the Suction Analogy to Vortex-Lift Estimates," NASA SP-347, Part II, pp. 985-1011, 1975.

[8] Scholz, N., "Kraft-und Druckverteilungsmessungen an Tragflächen kleiner Streckung," *Forschung, Auf Demgebiet Des Ingenieurwesens*, Vol. 16, No. 3, 1949-50, pp. 85-91.

[9] Kuhlman, J., "Load Distributions on Slender Delta Wings Having Vortex Flow," *Journal of Aircraft*, Vol. 14, July 1977, pp. 699-702.

[10] Davenport, E. E. and Huffman, J. K., "Experimental and Analytical Investigation of Subsonic Longitudinal and Lateral Aerodynamic Characteristics of Slender Sharp-Edge 74° Swept Wings," NASA TN D-6344, 1971.

[11] Ericsson, L. E. and Reding, J. P., "Nonlinear Slender Wing Aerodynamics," AIAA Paper 76-19, Washington, D.C., 1976.

[12] Manro, M. E., Manning, K.J.R., Hallstaff, T. H., and Rogers, J. T., "Transonic Pressure Measurements and Comparison of Theory to Experiment for an Arrow-Wing Configuration," NASA CR-2610, 1975.

[13] Wentz, W. J. Jr. and Kohlman, D. L., "Wind-Tunnel Investigations of Vortex Breakdown on Slender Sharp-Edged Wings," NASA CR-98737, 1968.

[14] Lambourne, N. C. and Bryer, D. W., "The Bursting of Leading-Edge Vortices – Some Observations and Discussion of the Phenomenon," British Aeronautical Research Council, R&M 3282, 1962.

[15] Lamar, J. E., "Longitudinal Aerodynamic Characteristics of 45° Swept Wings at Mach ~ 0," NASA TM X-73942, 1976.

[16] Bossel, H. H., "Vortex Breakdown Flowfield," *The Physics of Fluids*, Vol. 12, March 1969, pp. 498-508.

[17] Bossel, H. H., "Vortex Computation by the Method of Weighted Residuals Using Exponentials," *AIAA Journal*, Vol. 9, Oct. 1971, pp. 2027-2034.

[18] Raat, J., "Vortex Development and Breakdown," AIAA Paper 75-881, AIAA 8th Fluid and Plasma Dynamics Conference, Hartford, Conn., June 1975.